# Blow-Down Calibration of a Large 8 Path Ultrasonic Flow Meter under Quasi-Steady Flow Conditions

A. JOHNSON[1], E. HARMAN[2], and J. BOYD[1]
National Institute of Standards and Technology (NIST)
100 Bureau Drive Mail stop 8361
Gaithersburg, MD 20899
Aaron.Johnson@nist.gov

## ABSTRACT

We used an array of critical flow venturis (CFVs) in a blow-down facility to calibrate a large ($D$ = 89.5 cm) 8 path ultrasonic flow meter at atmospheric pressure. The calibration was performed with dry air spanning the flow range 2 kg/s to 36 kg/s. At the largest flows, pressure transients associated with the blow-down system resulted in quasi-steady flow conditions. The quasi-steady conditions were measured using a high speed data acquisition system that scanned 66 instruments (*i.e.*, pressure and temperature sensors) every 1.8 s. Corrections were made for thermal lag of the RTD temperature sensors, and for mass storage effects in the 230.3 $m^3$ connecting volume between the CFV array and the ultrasonic flow meter. The uncertainty of the calibration (with coverage factor $k$ = 2 corresponding to 95 % confidence level) ranged from 0.45 % to 0.58 %.

## INTRODUCTION

The *boot-strap method* has often been used by metrologist to facilitate the calibration of large flow meters [1, 2]. In this method several small flow meters are individually calibrated via a low flow primary standard, and then combined in parallel to calibrate a larger flow meter. Herein we used a parallel array of 8 critical flow venturis (CFVs) to calibrate a large 8 path ultrasonic flow meter (USM) with an inside diameter of $D_{USM}$ = 89.51 cm (35.24 inch). The 8 CFVs were mounted in parallel into a nozzle holder of diameter $D_1$ = 76 cm (30 inch). The nozzle holder was installed in a pipeline of the same diameter. Each of the 8 CFVs has a nominal throat diameter of $d_{th,nom}$ = 2.54 cm (1 inch) and is traceable to NIST's 26 $m^3$ *PVTt* standard [3, 4]. In this way the CFV array provided traceability to the SI unit of flow.

The CFV array exhausted into a large connecting volume (230.3 $m^3$) equipped with multiple flow conditioning devices. The large connecting volume was designed to reduce hydrodynamic and acoustic installation effects before the flow reached the downstream USM. The USM was calibrated in dry air[3] at 10 set points spanning the velocity range from 3.5 m/s to 57 m/s (11.5 ft/s to 187 ft/s) at an ambient pressure of approximately 84 kPa. The expanded uncertainty (*i.e.*, coverage factor of $k$ = 2) of the calibration factor is parabolic. It decreases from 0.56 % at 3.5 m/s to a minimum of 0.45 % at the velocity of 29 m/s and then increases to 0.58 % at the maximum velocity of 57 m/s.

The calibration was performed at the Colorado Engineering Experimental Station Incorporated (CEESI) using their blow-down facility shown in Fig. 1.[4] The source of flow was a manifold of high pressure (HP) collection vessels installed upstream of the CFV array. The HP valve shown in the figure was manually adjusted to maintain the pressure at the CFV array as steady as possible during each of the 10 set points. However, for these high flows (*i.e.*, 2 kg/s to 36 kg/s) only quasi-steady conditions could be realized, and the pressure at the CFV decreased by as much as 5 % during a set point. We compensated for these moderate flow transients 1) by applying the transient CFV methods established by Wright [5], 2) by accounting for the stored mass in the connecting volume [6], and 3) by correcting for thermal lag of resistance temperature detectors (RTDs).

Analogous to Wright's work, we used fast response pressure sensors (20 μs) to resolve the quasi-steady pressure transients and we used a heat exchanger (HX) to reduce temperature transients. Data was collected

[1] National Institute of Standards and Technology (NIST).

[2] Colorado Engineering Experimental Station Inc. (CEESI).

[3] Dew point temperature of -73.3 C (-100°F).

[4] Certain commercial equipment, instruments, or materials are identified in this report in order to specify the experimental procedure adequately. Moreover, the CFV array and all auxiliary measurements (*e.g.*, temperature and pressure) are traceable to NIST standards, and all data analysis was performed by NIST.

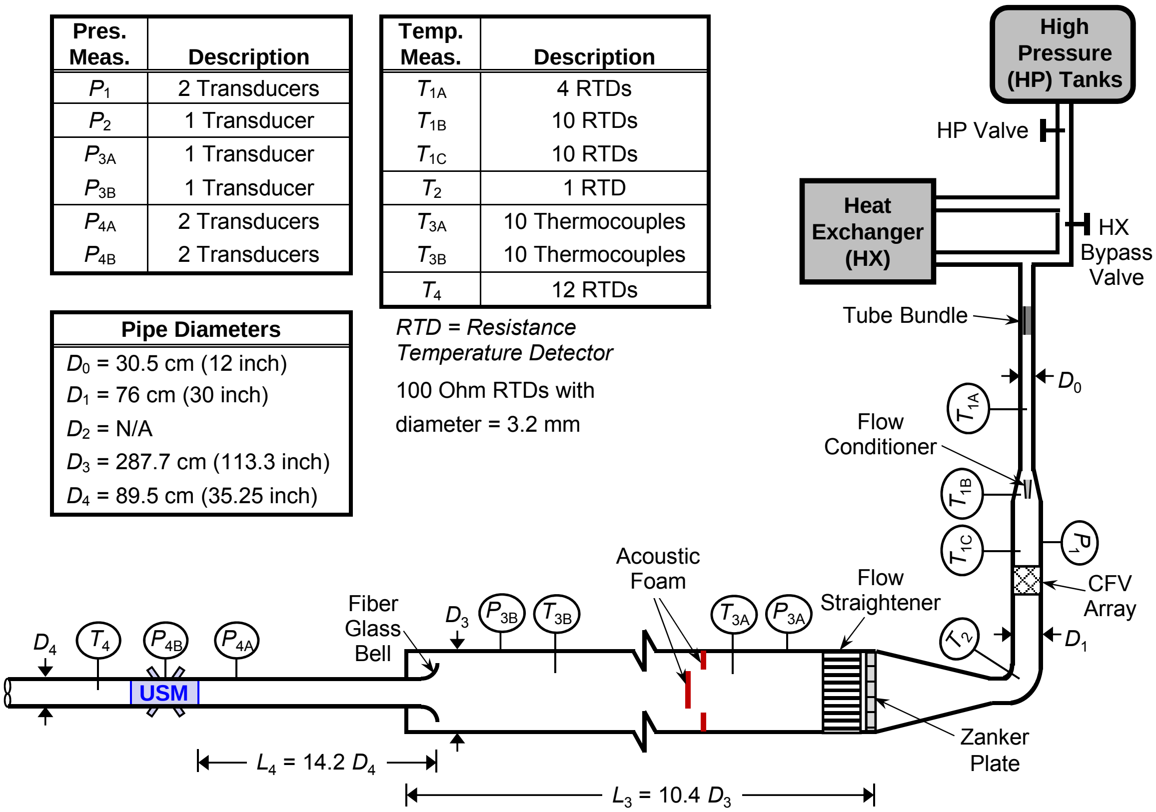


**Figure 1.** Schematic showing the CEESI blow-down facility used to calibrate the large 8 path USM

using a high speed data acquisition system that scanned 66 instruments (*i.e.*, pressure and temperature sensors) every 1.8 s. The calibration was performed on two occasions, first on May 5, 2012, and a second time on May 7, 2012 so that the reproducibility of the calibration factor could be determined. This manuscript presents the results and uncertainty of this blow-down calibration.

## DESCRIPTION OF BLOW-DOWN FACILITY

Figure 1 shows the key components of the CEESI blow-down facility. They include: 1) the array of high pressure (HP) collection tanks used to establish flow, 2) the heat exchanger (HX) used to heat the cold exhaust from the high pressure tanks to ambient temperature, 3) the NIST traceable CFV array used to determine the flow, 4) the connecting volume ($V_{cv} = 230.3$ m$^3$) consisting of the piping network from the exit of the CFV array to the USM, 5) the 8 path USM being calibrated, 6) the instrumentation used to measure pressure and temperature, and 7) various flow conditioning devices (*e.g.*, tube bundle, perforated plate conditioner, flow straightener, and fiber glass bell).

The blow-down facility was fabricated outdoors in order to accommodate its large size at a reasonable cost. Since the ambient temperature cannot be controlled, an open sided tent was used to shield the CFV array, the USM, and their auxiliary pressure and temperature sensors from the sun during calibration. In addition, to prevent errors attributed to thermal effects on the CFVs and USM, calibrations were performed during weather conditions when the skin temperature of the piping was close to the operating gas temperature.

The calibration began by opening the HP valve in Fig. 1 to ramp the pressure at the CFV array ($P_{CFV}$) to the first set point of 3700 kPa. This pressure set point was maintained as stable as possible during data collection. After completing measurements at the first set point, the HP valve was manually adjusted to the next set point at a lower pressure. This procedure was repeated until reaching the last set point of 250 kPa. The duration of each set point increased almost linearly with decreasing pressure, lasting 36 s at the highest pressure and increasing to 150 s at the lowest pressure. The total calibration lasted 1650 s.

The air temperature at the CFV array was controlled by mixing the cold exhaust from the HP tanks with hot air passing through the heat exchanger. The HX bypass valve shown in Fig. 1 diverts a fraction of flow to the heat exchanger where it was heated and then returned to the piping network to mix with the cold exhaust. An operator manually adjusted the valve during the calibration process to maintain the CFV array temperature ($T_{CFV}$) as stable as possible near the ambient temperature. Figure 2 shows the time history of $T_{CFV}$ denoted by the dashed line (----), and of $P_{CFV}$ denoted by the solid line (—). The groups of sequential pressure data points (◆) at the same nominal pressure correspond to the 10 series selected for processing or *set points*. The average CFV array mass flow ($\tilde{\dot{m}}_{array}$) was calculated at each set point using the averages of the respective pressure (◆) and temperature (▲) data points.

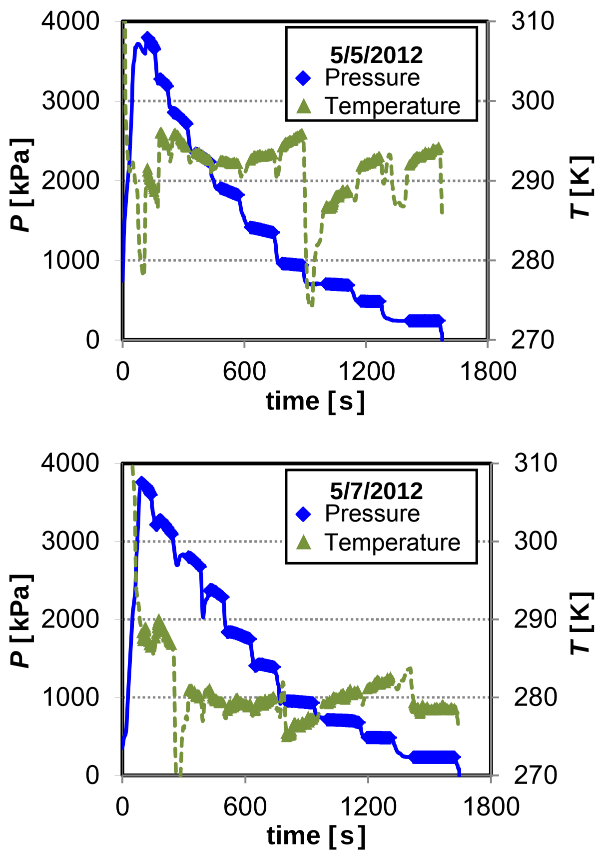


**Figure 2**. Time trace of the pressure ($P_{CFV}$) and temperature ($T_{CFV}$) upstream of the CFV array on 5/5/2012 and 5/7/2012.

The time-dependencies of $P_{CFV}$ and $T_{CFV}$ in Fig. 2 show the quasi-steady conditions during the calibration. The pressure decreased by as much as 5 % at the highest pressure set points (or highest flows) and by 1 % or less at the lowest pressure set points (or lowest flows). In spite of the heat exchanger, $T_{CFV}$ also varied during set points. On 5/5/2012 the temperature variation during the 10 set points ranged from 0.13 K to 0.87 K while on 5/7/2012 the temperature variation ranged from 0.25 K to 0.98 K.[5]

The largest temperature transients occurred during transitions between set points as shown in Fig. 2. The temperature sharply decreases during the transitions to the lower pressure set points due to adiabatic cooling. However, $T_{CFV}$ quickly recovers as the HX bypass valve was manually adjusted to control the temperature. Excluding set points #1, #2, and #7 on 5/5/2012, and set points #1 and #3 on 5/7/2012, the transitional temperature variations were generally less than 3 K. The large initial transients associated with set point #1 were caused by the pressure ramp-up during the startup of the blow-down system. Much of the remaining temperature transients resulted from the limited ability of the operator to control the HX bypass valve and could be reduced by automating the valve's operation.

# FLOW MEASUREMENT AT THE CFV ARRAY

*Installation of CFV Array*

Figure 3 is a photograph of the CFV array installation. Flow exiting the heat exchanger enters a straight section of piping with a diameter of $D_0$ = 30.5 cm. A tube bundle at the entrance of the pipe reduces swirl introduced from the upstream elbow. At the end of this pipe section, a transition section increases the diameter to $D_1$ = 76 cm. A flow conditioner installed in the interior of the transition section reduces jetting effects [2] in the larger piping section as shown in the figure. The CFV array was installed in a flange that holds up to 21 CFVs. The CFV holder was installed in a pipe spool of an ultrasonic flow meter.[6] For this calibration we used only 8 of the possible 21 CFVs.

The mass flow through the CFV array was determined by

$$\dot{m}_{array} = \frac{P_0 C^* \sqrt{\mathcal{M}} A_{array} C_{d,array}}{\sqrt{R_u T_0}}, \qquad (1)$$

where $P_0$ and $T_0$ are the respective stagnation pressure and temperature [7], $C^*$ is the real gas critical flow factor, which is computed at the stagnation

[5] Temperature variations during a set point are defined as the standard deviation of the temperature data points (▲).

[6] The ultrasonic flow meter was not used in this work, but in the future we hope to use the ultrasonic flow meter to determine the temperature from the speed of sound.

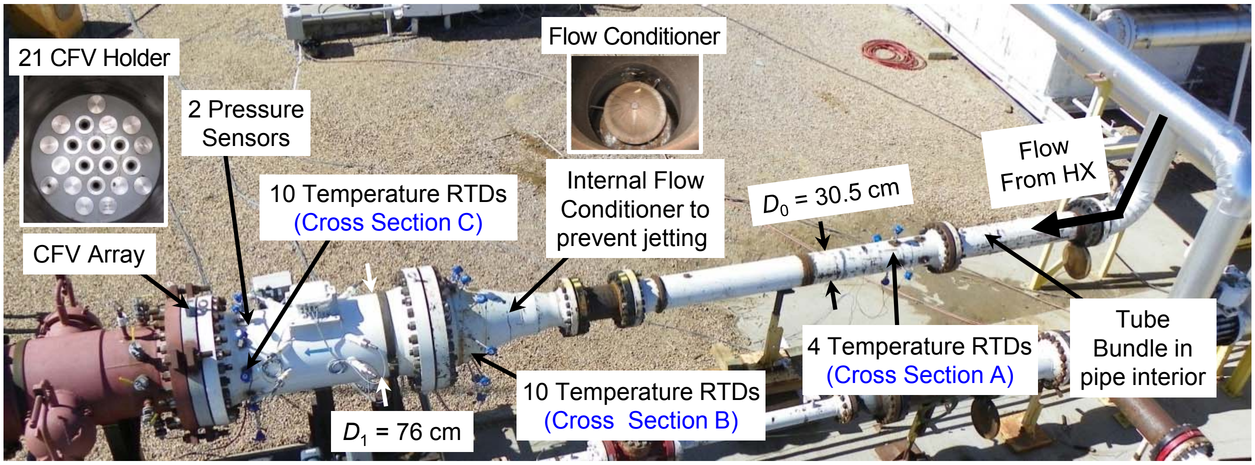


**Figure 3.** Installation of CFV Array (During the calibration the setup is covered with tarp)

conditions $P_0$ and $T_0$ using the REFPROP 9.0 thermodynamic data base [8], $\mathcal{M}$ = 28.9655 kg/kmol is the molar mass of dry air [9], $R_u$ = 8314.472 J/(kmol·K) is the universal gas constant [10], and the discharge coefficient for the CFV array is defined by

$$C_{d,array} = \frac{\sum_{n=1}^{8} C_{d,n} A_{th,n}}{\sum_{n=1}^{8} A_{th,n}} = \frac{\sum_{n=1}^{8} C_{d,n} A_{th,n}}{A_{array}}, \quad (2)$$

where $C_{d,n}$ is the discharge coefficient of the n$^{th}$ NIST traceable CFV, and $A_{th,n} = \pi d_{th,n}^2 / 4$ is the throat area of the n$^{th}$ CFV.

*Temperature Measurements upstream of CFV Array*
As shown in Fig. 3 the temperature was measured at three cross sections upstream of the CFV array labeled A, B, and C. At each cross section the temperature was determined by averaging the RTDs installed around the pipe circumference. All of the RTDs have a resistance of 100 ohms and a probe diameter of 3.2 mm. At cross section A (the smallest pipe diameter) the average temperature ($T_{1A}$) was determined using 4 RTDs. The temperature in the reducer at cross section B ($T_{1B}$) and the temperature immediately upstream of the CFV array at cross section C ($T_{1C}$) were both determined using 10 RTDs. These measurements were used to account for temperature non-uniformities in the average CFV array temperature, and to quantify the uncertainty attributed to spatial sampling errors.

In addition to spatial sampling errors the time response of the RTDs must also be considered. The slow moving air upstream of the CFV array results in poor heat transfer between the RTDs and the air, causing the RTD temperature measurements to lag behind the transient air temperature. The estimated air speed is 11 m/s in the smaller diameter piping at cross section A, and only 2 m/s in larger piping at cross section C. Therefore, the time response of the RTDs installed at cross section C was slower than the RTDs at cross section A.

Time response corrections were made using a first order heat transfer model

$$\hat{T}_n = \tau_n \frac{dT_n}{dt} + T_n \quad (3)$$

which is based on an energy balance of the convected heat transfer from the RTD to the air stream [11]. Here, $T_n$ is the calibrated temperature output of the RTD, $\hat{T}_n$ is the *time response corrected temperature*, $\tau_n$ is the time constant of the RTD, and the subscript "n" corresponds to the measurement cross section (*e.g.*, 1A, 1B, 1C). The derivative term is calculated using a 2$^{nd}$ order finite difference [12]. Self-heating effects are small and have been omitted in the model, but are included in the uncertainty budget. The time response corrected CFV array temperature is[7]

$$\hat{T}_{CFV} = \left(\hat{T}_{1A} + \hat{T}_{1B} + \hat{T}_{1C}\right)/3 \quad (4)$$

where $\hat{T}_{1A}$, $\hat{T}_{1B}$, and $\hat{T}_{1C}$ are the time response corrected temperature measurements at the respective cross sections. The average temperature

[7] In applications with significant temperature gradients the temperature should be measured as close as possible to the CFV inlet (*i.e.*, at cross section C only). In this case, however, cross sections A and B are included in determining $T_{CFV}$ (see Eq. 4) because these RTDs have better time response than those at cross section C.

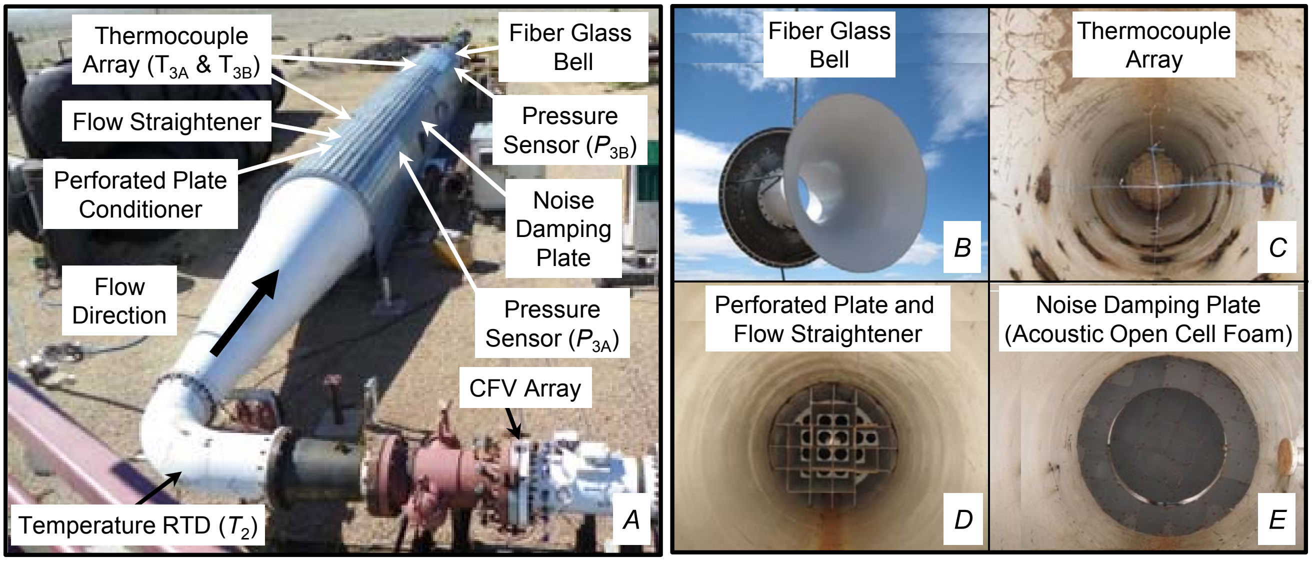


**Figure 4.** Pictures showing flow conditioning and the pressure and temperature instrumentation used in the connecting volume.

is used as The RTD time constant specified in Eq. (3) was calculated using an approach explained later in the manuscript. The measured pressure ($P_{\rm CFV}$) and temperature ($\hat{T}_{\rm CFV}$) are used to compute the stagnation conditions using the following expressions

$$P_0 = P_{\rm CFV}\left[1+\left(\frac{\gamma-1}{2}\right)M^2\right]^{\gamma/\gamma-1}, \qquad (5a)$$

$$T_0 = \hat{T}_{\rm CFV}\left[1+(1-r)\left(\frac{\gamma-1}{2}\right)M^2\right] \qquad (5b)$$

where $\gamma = C_p/C_v$ is the ratio of constant pressure to constant volume specific heats, $r = 0.75$ is the assumed value of the recovery factor which accounts for viscous heating of the gas as it stagnates against the temperature probe, and $M$ is the Mach number in the approach piping which is calculated using the following low Mach number approximation [2]

$$M = \frac{1}{\beta^2}\left(\frac{2}{\gamma+1}\right)^{\frac{\gamma-3}{2\gamma-2}}\left[1-\sqrt{1-2\beta^4\left(\frac{2}{\gamma+1}\right)^{\frac{2}{\gamma-1}}}\right], \qquad (6)$$

where $\beta = d_{\rm eff}/D_1$ and $d_{\rm eff} = \sqrt{4A_{\rm array}/\pi}$.

## FLOW CONDITIONING AND STORED MASS IN THE CONNECTING VOLUME

The large connecting volume (230.3 m$^3$) between the CFV array and the USM is designed to reduce velocity and temperature distortions created by the exhaust of the CFV array. Figure 5 shows the connecting volume and the various flow conditioning devices used to produce a well-conditioned velocity and temperature field at the USM. The temperature of the cold, supersonic jet from the 8 CFVs increases as it decelerates in the downstream piping. The perforated plate flow conditioner in the large constant diameter section ($D_3$ = 2.877 m) helps decrease profile asymmetries, while the flow straightener immediately downstream reduces swirl. A noise damping plate made of acoustic open cell foam attenuates ultrasonic noise before the flow enters the toroidal shaped fiber glass bell. The geometry of the fiber glass bell accelerates the flow and results in a nearly uniform velocity profile at its exit plane.

Temperature and pressure measurements are made throughout the connecting volume in the locations shown in Figs. 1 and 4. The pressure and temperature measurements along with the equation of state for dry air, and the size of the connecting volume ($V_{\rm cv}$ = 230.3 m$^3$) are used together to determine the mass in the connecting volume during a set point. Since the mass entering and exiting the connecting volume differs during a set point, the mass stored in the connecting volume varies with time. The time-averaged rate of mass change ($d\tilde{M}_{\rm cv}/dt$) in the connecting volume is the mass change in the connecting volume during a set point divided by the collection time

$$\frac{d\tilde{M}_{\rm cv}}{dt} = \frac{M_{\rm cv,f}-M_{\rm cv,i}}{\Delta t} = V_{\rm cv}\left(\frac{\rho_{\rm cv,f}-\rho_{\rm cv,i}}{\Delta t}\right), \qquad (7)$$

where $\rho_{\rm cv,i}$ and $\rho_{\rm cv,f}$ are the respective densities of

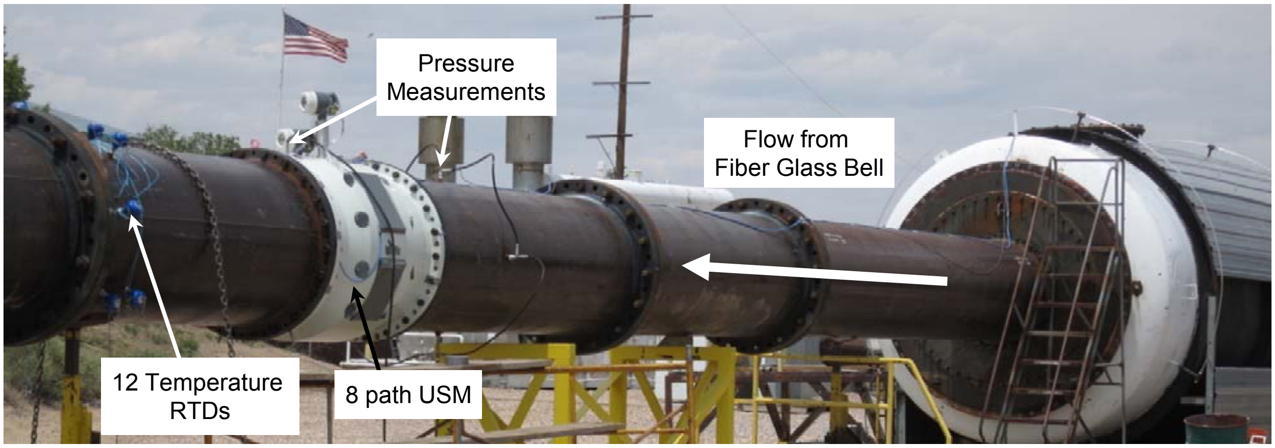


**Figure 5.** Picture of 8 path USM installation.

dry air at the beginning and ending of a set point. Mass storage effects accounted for as much as 0.34 % of the mass flow at the USM.

Prior to calibrating the USM we used a density decay test to check the connecting volume for leaks. We installed blind flanges just upstream of the CFV array and downstream of the USM. The sealed connecting volume was then pressurized to 9.7 kPa above ambient. The pressure and temperature were recorded at approximately 37 s intervals over a period of 2268 s. The mass at each time stamp was determined by multiplying the density (determined via the pressure and temperature measurements) by the size of the connecting volume. The leak rate is the slope of the mass verses time which was determined by linear regression to be $1.7 \times 10^{-3}$ kg/s. In the worst case (*i.e.*, the lowest flow) the leak accounts for 0.073 % of the CFV array mass flow.[8]

# USM CALIBRATION RESULTS

*Pre-Calibration Testing*

Before installing the USM in the calibration facility we compared its measured speed of sound ($a_{\mathrm{meter}}$) with the calculated thermodynamic speed of sound under zero-flow conditions. The USM was sealed using two blind flanges, one on either end, and moved to a thermostatted room. We pressurized the USM with air (at a dew point of 260.9 K) to 166.53 kPa, and measured the average air temperature with 8 RTDs. Four RTDs were installed in each blind flange and configured vertically along the flange diameter. The standard deviation of the thermodynamic temperature measured by the 8 RTD was 0.039 %. The thermodynamic speed of sound ($a_{\mathrm{REFPROP}}$) was calculated using the REFPROP database for air at the measured pressure, temperature, and moisture content. The measured and calculated sound speeds were in good agreement with $a_{\mathrm{meter}} > a_{\mathrm{REFPROP}}$ by only 0.043 %. We found differences of the same magnitude and polarity during flow calibrations. On 5/5/2012 and 5/7/2012 the differences were 0.042 % and 0.051 %, respectively.[9]

In this work the zero-flow (ZF) sound speed ratio, defined by

$$\xi = \left[\frac{a_{\mathrm{REFPROP}}}{a_{\mathrm{meter}}}\right]_{\mathrm{ZF}}, \tag{8}$$

was multiplied by the sound speeds measured by the USM during flow calibrations. In this way the sound speeds measured by the USM were calibrated to correspond with the thermodynamic temperature and pressure via the REFPROP database [8]. Moreover, these corrected sound speeds, herein referred to as the *adjusted USM sound speed* ($a'_{\mathrm{meter}} = \xi\, a_{\mathrm{meter}}$), can be used to back calculate the temperature [13]. We implemented this method at the lower air velocities where RTD temperature measurements are adversely impacted by thermal lag.

After installing the 8 path USM in the blow-down facility a preliminary test was performed at the maximum velocity of 57 m/s (187 ft/s) to assess the performance of two sets of USM transducers with

8 During the calibration the difference between the ambient pressure and the pressure in the connecting volume never exceeded 1 kPa. Thus, the estimated leak rate is the maximum possible.

9 The first 2 set points were omitted due to the large spatial sampling uncertainty in the measured temperature.

frequencies of 80 kHz and 135 kHz, respectively. During the test, the 80 kHz transducers were installed in 4 of the 8 USM paths, and 135 kHz transducers were installed in the remaining 4 paths. Because the signal to noise ratio was better for the 80 kHz the manufacturer replaced the 135 kHz transducers with 80 kHz transducers. Therefore, all 8 paths of the USM were equipped with 80 kHz transducers for the calibration. In addition, the manufacturer adjusted several of the USM electronic settings. For example, the measuring rate was set to 15 samples per second, and the average buffer was set to 30 samples thereby giving a response time of 2 seconds.

*Installation of the 8 Path USM*

The USM was installed in a straight section of piping located a distance of $L_4$ = 14.2 $D_4$ downstream from the fiber glass bell as shown in Fig. 1. The pressure ($P_{USM}$) was measured at two locations, just upstream of the USM, and at a port on the USM meter body as shown in Fig. 5. The temperature ($T_{USM}$) was measured using 12 RTDs installed downstream of the USM to avoid disturbing the velocity profile at the USM's inlet. The calibrated temperature output was corrected for thermal lag using Eq. (3). We calculated the air density ($\rho_{USM}$) using the REFPROP database [8], the average pressures ($P_{USM}$), and the time-response-corrected temperature measurements ($\hat{T}_{USM}$).

*Calibration Parameters*

Conservation of mass was used to determine the velocity at the USM ($v_{NIST}$). The time-averaged mass flow at the USM equals the mass flow from the CFV array entering the connecting volume minus the average rate of mass stored in the connecting volume

$$\tilde{\dot{m}}_{USM} = \tilde{\dot{m}}_{array} - d\tilde{M}_{cv}/dt\,, \tag{9}$$

The average USM velocity during a set point is the time-averaged mass flow divided by the density and cross sectional area

$$v_{NIST} = \frac{\tilde{\dot{m}}_{array} - d\tilde{M}_{cv}/dt}{\rho_{USM} A_{USM}}, \tag{10}$$

where $\tilde{\dot{m}}_{array}$ is given by Eq. (1), $d\tilde{M}_{cv}/dt$ is given by Eq. (7) and $A_{USM} = \pi D_{USM}^2/4$ is the cross sectional area of the USM.

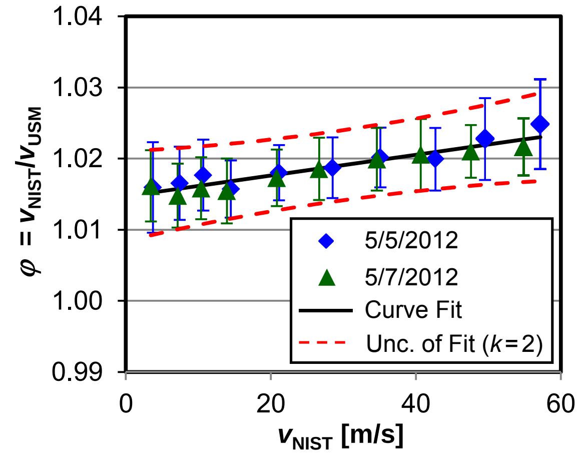


**Figure 6.** Calibration data of 8 Path USM

The USM calibration factor is the ratio of the NIST measured velocity and the velocity reported by the USM

$$\varphi = \frac{V_{NIST}}{V_{meter}}. \tag{11}$$

Figure 6 shows the calibration factor plotted against the NIST measured velocity for the datasets obtained on 5/5/2012 (◆) and 5/7/2012 (▲). The error bars on the calibration data were determined by applying the propagation of uncertainty to the calibration factor expressed in Eq. (11) [14, 15]. We fitted a polynomial to the velocity-dependent ($\varphi_{FIT}$) calibration data. The polynomial is plotted as solid curve (——), and its expanded uncertainty is denoted by the dashed lines (- - -). The polynomials used for the curve fit and its expanded uncertainty (expressed in percent) are given in Eq. (12a) and (12b) respectively

$$\varphi_{FIT} = a_0 + a_1\left(\frac{V_{NIST}}{V_{ref}}\right) + a_2\left(\frac{V_{NIST}}{V_{ref}}\right)^2, \tag{12a}$$

$$\frac{U_e(\varphi_{FIT})}{\varphi_{FIT}} = b_0 + b_1\left(\frac{V_{NIST}}{V_{ref}}\right) + b_2\left(\frac{V_{NIST}}{V_{ref}}\right)^2, \tag{12b}$$

where $V_{ref} = 1$ m/s and the fit coefficients are given in Table 1. The standard deviation of the residuals from $\varphi_{FIT}$ was 0.00087 and we use it as the measure of the reproducibility of the calibration.

**Table 1.** Fit Coefficients for Eq. (12a) and (12b)

| $a_0$ | $a_1$ | $a_2$ |
|---|---|---|
| 1.0147 | 0.000146 | 0 |
| $b_0$ | $b_1$ | $b_2$ |
| 0.6 | -0.0098 | 0.000166 |

The calibration results showed that the reported USM velocity ( $V_{meter}$ ) is offset nearly 1.9 % below the NIST velocity ( $V_{NIST}$ ). Additionally, the calibration data had a positive slope that spanned 0.77 % over the velocity range. The slope of the calibration data and the size of the offset were both unexpected. Several diagnostics of the USM were checked to try to resolve whether the flow meter or the calibration was responsible for these unexpected results.

The USM diagnostics (*e.g.*, symmetry factor, turbulence levels, speed of sound, and signal to noise) were found to be within the normal tolerances set by the manufacturer. The profile factor (*i.e.*, the ratio of the 4 inner chords with the 4 outer chords of the 8 path USM) was also within normal tolerances; however, the measured profile factors indicated a nearly flat velocity profile. This flat profile was caused by flow acceleration through the upstream fiber glass bell. Computational fluid dynamic simulations of the flow through the fiber glass bell also indicated a flat velocity profile [16]. Although the USM settings could be adjusted to compensate for profile effects, which would potentially linearize the data, we opted not to alter the USM profile settings. Instead the effects of the flat velocity profile are accounted for in the calibration curve shown in Fig. (6). Given that the same fiber glass bell and downstream piping will be used with the USM in flow measurement applications, the velocity profile will also be nearly the same. As such, uncertainty sources attributed to velocity profile are fully correlated and do not contribute to the uncertainty.

## TIME RESPONSE OF RTD TEMPERATURE MEASUERMENTS

At velocities less than 21 m/s the response times of the RTDs at the USM were too slow to characterize the temperature transients. For these low velocities we back calculated the thermodynamic temperature using the adjusted USM sound speed ( $a'_{meter}$ ). The adjusted sound speed was converted to temperature ( $T'_{meter}$ ) using the REFPROP database [8] and the measured pressure.

*Estimating the RTD time constant at the USM*

We estimated the time constants of the RTDs installed at the USM ( $\tau_{RTD}$ ) by fitting their measured temperature ( $T_{USM}$ ) to Eq. (3). The time constant was determined for the last 5 set points for air velocities ranging from 3.5 m/s to 21 m/s. At each set point $\tau_{USM}$ was determined such that the L2-norm of the difference between $\hat{T}_{USM}$ and $T'_{meter}$ was minimized. Here, the L2-norm is given by

$$L2\text{-norm} = 100\frac{\left[\sum_{n=1}^{N}\left(\hat{T}_{USM,n} - T'_{meter,n}\right)^2\right]^{1/2}}{\frac{1}{N}\sum_{n=1}^{N}T'_{meter,n}} \qquad (13)$$

where $N$ is the number of data points for the set point. The time response corrected RTD temperature ( $\hat{T}_{USM}$ ) was calculated iteratively by solving the left hand side of Eq. (3) at the measured $T_{USM}$ and guessed values of $\tau_{USM}$ until the L-2norm is minimized. Figure 7 shows the good agreement between $\hat{T}_{USM}$ and $T'_{meter}$ at the converged values of $\tau_{USM}$ for air velocities of 3.44 m/s and 13.9 m/s, respectively.

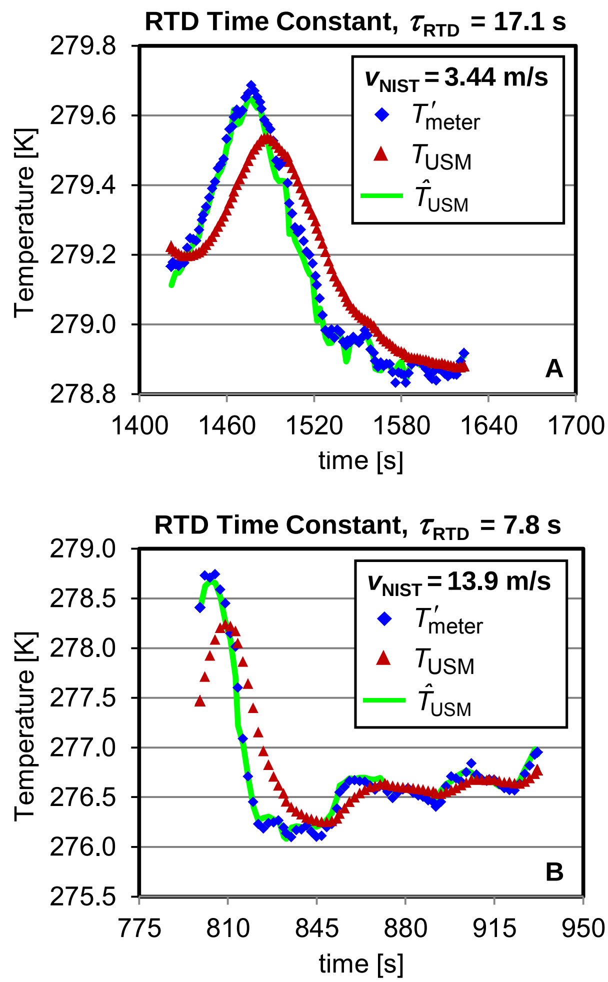


**Figure 7.** Compares $T'_{meter}$ (the adjusted USM temperature) with $T_{USM}$ (the calibrated RTD temperature), and $\hat{T}_{USM}$ (the time response corrected RTD temperature calculated using Eq. 3 at the specified time constant).

*Estimating the RTD time constants at the CFV array*

The make and model of the RTDs at the USM and at the CFV array are identical. Provided the heat transfer conditions are equivalent at the USM and at CFV array, the time constants at both locations will also be the same. Since forced convection is the dominant mode of heat transfer, the time constants at the USM and at the CFV array are equal when the Reynolds numbers[10] (based on the RTD probe diameter) are the same. Therefore we estimated the RTD time constants in the pipe sections upstream of the CFV array (*i.e.*, $\tau_A$, $\tau_B$, and $\tau_C$) by linearly interpolating the RTD time constant at the USM at matching Reynolds numbers. For cases where the RTD Reynolds number at the CFV array exceeded the maximum Reynolds number at the USM we used a time constant of 2 s.

# UNCERTAINTY ANALYSIS

The uncertainty of the blow-down calibration is based on the method of propagation of uncertainty [14, 15]. Applying this method to Eq. (11) results in the following generic expression

$$\frac{U_e(\varphi)}{\varphi} = k\left[\begin{array}{l}\sum_{i=1}^{N} S_i^2\left(\frac{u(x_i)}{x_i}\right)^2 \\ +2\sum_{i=1}^{N-1}\sum_{j=i+1}^{N} S_i S_j r_{ij}\left(\frac{u(x_i)}{x_i}\right)\left(\frac{u(x_j)}{x_j}\right) \\ +\sigma_{\mathrm{Repeat}}^2+\sigma_{\mathrm{Rprd}}^2\end{array}\right]^{1/2} \quad (14)$$

where $U_e(\varphi)/\varphi$ is the relative, expanded uncertainty of the calibration factor at the 95 % confidence level, $x_i$'s are the input quantities or dependent variables of $\varphi$, $S_i = x_i/\varphi(\partial\varphi/\partial x_i)$ is the normalized sensitivity coefficient for the i$^{th}$ input quantity, $r_{ij}$ is the degree of correlation between input quantities $x_i$ and $x_j$, $u(x_i)/x_i$ is the relative uncertainty of $x_i$ at the 68 % confidence level, $k = 2$ is the coverage factor, $\sigma_{\mathrm{Repeat}}$ is the repeatability (*i.e.*, the standard deviation of the mean of measured $\varphi$ values during a set point), and $\sigma_{\mathrm{Rprd}}$ is the reproducibility of the calibration data from 5/5/2012 and 5/7/2012.

Table 2 provides an itemized list of the relevant uncertainty components for data taken on 5/7/2012 at an air velocity at the USM of $V_{\mathrm{NIST}}$ = 34.4 m/s. The table includes a brief explanation of how all of the uncertainty components were estimated. The abbreviated titles in the heading of the table, "**Input. Quant.**", "**Rel. Unc.**", "**Sen. Coeff.**", "**Perc. Contrib.**", and "**Unc. Type**", denote the following: (1) Input Quantity, (2) standard relative uncertainty; (3) normalized sensitivity coefficient; (4) percent contribution of a single component to the overall uncertainty; and (5) the type of uncertainty either Type A or Type B, respectively. The **boldface headings** are the primary variables comprising $V_{\mathrm{NIST}}$ and are specified in Eq. (9). The *italicized entries* directly below the **boldface headings** itemize the uncertainty components of each primary variable.

The expanded uncertainty for this particular velocity ($V_{\mathrm{NIST}}$ = 34.4 m/s) was $U_e(\varphi)$ = 0.44 %. The largest uncertainty sources are the determination of the air density at the USM, and the mass flow measurement made by the CFV array. The uncertainty of the air density at the USM comprises 43.7 % of the uncertainty budget while the uncertainty in the mass flow through the CFV array contributes 30.9 %. The large uncertainty in the air density corresponds to the large uncertainty in the USM temperature and is mainly attributed to spatial sampling errors. The uncertainty in the CFV array mass flow is mainly attributed to the uncertainty of the discharge coefficient of the CFVs.

For this calibration the uncertainty varied as a function of the velocity at the USM. In particular, the lowest uncertainties were realized at intermediate velocities while the largest uncertainties occurred at both the low and high velocities. At high flows the uncertainty in the USM temperature is significant while at the low flows mass storage effects makeup a larger fraction of the total flow. Figure 6 shows the parabolic uncertainty curve and Eq. (11b) is a curve fit of the expanded uncertainty of the calibration factor (expressed in percent) as a function of $V_{\mathrm{NIST}}$.

# SUMMARY AND CONCLUSIONS

A blow-down facility was used to calibrate a large diameter ($D$ = 89.5 cm) ultrasonic flow meter (USM) in dry air over a velocity range from 3 m/s to 57 m/s. The calibration was performed on two occasions, first on 5/5/2012, and a second time on 5/7/2012. The expanded uncertainty of the calibration factor ranged from 0.45 % to 0.58 % depending on the velocity. The reference flow standard was an array of 8 critical flow venturis (CFVs) installed upstream of the USM. Each of the CFVs had a nominal throat diameter of 2.54 cm and was traceable to NIST's primary flow standards.

[10] A dimensionless parameter equal to the product of the air density, fluid velocity, and RTD diameter, divided by the dynamic viscosity.

**Table 2**. Uncertainty budget of the calibration factor in Eq. (10) at $V_{NIST}$ = 34.4 m/s for data collected on 5/7/2012.

| Input Variables, ($x_i$) | Input Quant. $x_i$ [SI] | Rel. Unc. [u($x_i$)/$x_i$] [%,$k$ = 1] | Sens. Coeff. $S_i$ [ ] | Perc. Contrib. [%] | Unc. Type [A or B] | Comments [ ] |
|---|---|---|---|---|---|---|
| **CFV Mass Flow, $\dot{m}_{array}$** | **23.06 kg/s** | **0.122** | **1** | **30.9** | **B** | a |
| *Discharge Coefficient,* ($C_{d,Array}$) | 0.9948 | 0.10 | 1 | 20.7 | B | b |
| *Stagnation Pressure,* ($P_0$) | 2342.5 kPa | 0.030 | 1 | 1.9 | B | c |
| *Stagnation Temperature,* ($T_0$) | 279.87 K | 0.081 | -0.5 | 3.4 | B | d |
| *Critical Flow Factor,* ($C^*$) | 0.6927 | 0.035 | 1 | 2.5 | B | e |
| *Throat Area of CFVs,* ($A_{array}$) | 40.51 $cm^2$ | 0.034 | 1 | 2.4 | B | f |
| **Rate of Stored Mass in Connecting Volume, ($d\tilde{M}_{cv}/dt$)** | **0.0133 kg/s** | **0.041** | **1** | **3.6** | **B** | g |
| *Connecting Volume Size,* ($V_{cv}$) | 230.3 $m^3$ | 10 | $-6 \times 10^{-4}$ | 0.1 | B | h |
| *Pressure* | N/A | 0.023 | 1 | 1.1 | B | i |
| *Temperature* | N/A | 0.034 | 1 | 2.4 | B | j |
| *Compressibility Factor* | N/A | 0.000 | 1 | 0.0 | B | k |
| *Collection Time Interval,* ($\Delta t$) | 67 s | 1.5 | $-6 \times 10^{-4}$ | 0.0 | B | l |
| **Bore Diameter of USM, ($A_{USM}$)** | **0.629 $m^2$** | **0.016** | **1** | **0.5** | **B** | m |
| **Density of air at USM, ($\rho_{USM}$)** | **1.0591 $kg/m^3$** | **0.145** | **1** | **43.8** | **B** | n |
| *USM Temperature,* ($T_{USM}$) | 276.71 K | 0.136 | 1 | 38.3 | B | o |
| *USM Pressure,* ($P_{USM}$) | 84.086 kPa | 0.051 | 1 | 5.4 | B | p |
| *USM Compressibility Factor,*($Z_{USM}$) | 0.9996 | 0.005 | 1 | 0.1 | B | q |
| **Fluid Constants** | **N/A** | **0.002** | **1** | **0.0** | **B** | r |
| *Universal Gas Constant,* ($R_{univ}$) | 8.31447 J/(K·mol) | 0.000 | 0.5 | 0.0 | B | s |
| *Molar Mass*, ($\mathcal{M}$) | 28.9655 g/mol | 0.003 | -0.5 | 0.0 | B | t |
| Leak Flow | 0.0023 kg/s | 0.006 | 1 | 0.1 | B | u |
| Repeatability, ($\sigma_{Repeat}$) | $5.4 \times 10^{-4}$ | 0.053 | 1 | 5.8 | A | v |
| Reproducibility, ($\sigma_{Rprd}$) | $8.8 \times 10^{-4}$ | 0.086 | 1 | 15.3 | A | w |
| **Expanded Uncertainty, $U_e$ = 0.44 %** | | | | **100** | | |

[a] Propagation of Uncertainty of Eq (1)
[b] NIST traceable calibration of CFVs
[c] Calibration records
[d] Calibration records, time response, and spatial sampling errors
[e] Uncertainty of $C^*$ is highly correlated between CFV calibration and application (*i.e.*, same gas, $T_0$, $P_0$, and REFPROP database)
[f] Thermal expansion of CFV throat during calibration attributed to estimated 17.5 K change of throat (rectangular distribution)
[g] Propagation of uncertainty of Eq. (7)
[h] Specifications of standard piping sections and dimensional measurments
[m] Data acquisition system (rectangular distribution)
[n] Propagation of uncertainty of equation of state (Note: temperature measurement account for largest source of uncertainty)
[o] Cal. Records, Time Response, & Spatial Sampling Errors
[p] Cal. Records & Spatial Sampling Errors
[q] REFPROP Data Base [8]
[r] Combined unc. of $R_{univ}$ & $\mathcal{M}$
[s] Reference [10]
[t] Reference [4]
[u] Leak rate measured via a density decay test made prior to calibration
[v] Standard deviation of the mean of the measured calibration factor during a set point
[w] Curve fit residuals

The blow-down facility used a manifold of high pressure tanks as the source of flow. A manually operated control valve was used to set the pressure (and thereby the flow) upstream of the CFV array. The calibration included a total of 10 pressure set points, starting at the maximum pressure of 3700 kPa, and decreasing at each successive set point until reaching the minimum pressure of 250 kPa. A heat exchanger was used to compensate for adiabatic cooling effects that occurred between set points when the manual valve was adjusted to decrease the pressure.

For these large flows the highest pressures could only be maintained for short time intervals. The duration of the highest pressure set point lasted only 36 s, but increased to 150 s at the lowest pressure. These short durations coupled with manual pressure control did not provide sufficient time to establish steady state conditions during set points. The pressure dropped by as much as 5 % and temperature varied by as much as 0.9 K during set points. To account for transients in the pressure and temperature we 1) used pressure sensors with a 20 ms time constant, 2) made corrections for mass storage effects in the connecting volume between the CFV array and the ultrasonic flow meter, 3) made time response corrections for the temperature measurements both at the CFV array and at the ultrasonic flow meter, and 4) used a high speed data acquisition system that scans 66 instruments (*i.e.*, pressure and temperature sensors) every 1.8 s. In addition, the connecting volume was used to hydrodynamically and acoustically condition the CFV exhaust in order to minimize installation effects at the USM.

# REFERENCES


[1] Johnson, A. N. and Kegel, T. ***Uncertainty and Traceability for the CEESI Iowa Natural Gas Facility***, J. Res. Natl. Inst. Stand. Technol., 109, pp. 345-369 (2004).

[2] Johnson, A. N., ***Natural Gas Flow Calibration Service (NGFCS)***, NIST Special Publication 250-1081, National Institute of Standards and Technology, Gaithersburg, MD, (2008).

[3] Johnson, A. N. and Wright, J. D., ***Gas Flowmeter Calibrations with the 26 $m^3$ PVTt Standard***, NIST Special Publication 250-1046, 2006.

[4] Johnson, A. N., Wright, J. D., Moldover, M. R., and Espina, P. I., ***Revised Uncertainty Analysis of the 26$m^3$ PVTt Flow Standard***, Proceedings of $6^{th}$ ISFFM Conference, Querétaro, Mexico., 2006

[5] Wright, J. D., ***Performance of Critical Flow Venturis under Transient Conditions*****,** Measurement Science & Technology, 2010.

[6] Pope, J. and Wright, J. D., ***Performance of Coriolis Meters in Transient Gas Flows*****,** Flow Measurement and Instrumentation, Submitted 2013.

[7] Wright, J. D., ***Blow-Down Tests Confirm Accurate Critical Flow Venturi Measurements During Transients*****,** Proceedings of the International Symposium for Fluid Flow Measurement (ISFFM), Anchorage, AK, 2009.

[8] Lemmon E. W., Huber M. L., and McLinden M. O., ***NIST Standard Reference Database 23: Reference Fluid Thermodynamic and Transport Properties-REFPROP, Version 9.0*** National Institute of Standards and Technology, Standard Reference Data Program, Gaithersburg, 2007.

[9] Wright, J. D., ***Blow-Down Tests Confirm Accurate Critical Flow Venturi Measurements During Transients*****,** Proceedings of the International Symposium for Fluid Flow Measurement (ISFFM), Anchorage, AK, 2009.

[10] Moldover M. R., Trusler J. P. M., Edwards T. J., Mehl J. B., and Davis R. S., ***Measurement of the Universal Gas Constant R Using a Spherical Acoustic Resonator***, **J. Res. Natl. Inst. Stand. Technol**. 93, (2), 85 to 143, (1988).

[11] **DeWitt D. P., Bergman, T. L., and Lavine, A. S.,** ***Fundamentals of Heat and Mass Transfer $6^{th}$ Ed.*****,** John Wiley & Sons, **2007**.

[12] Press, W. H., Flannery, B. P., Teukolsky, S. A., Vetterling, W. T., ***Numerical Recipes in FORTRAN 77: The Art of Scientific Computing $2^{nd}$ Ed.***, Cambridge University Press, 1992.

[13] Lansing, J., ***Smart Monitoring and Diagnostics for Ultrasonic Gas Meters***, $18^{th}$ North Sea Flow Meausrement Worshop, 2000.

[14] Coleman, H. W, and Steele, W. G., ***Experimetation and Uncertianty Analysis for Engineers***, Johm Wiley and Sons, Inc. New York, 1989.

[15] Taylar, B. N., and Kuyatt C. E., ***Guidelines for the Evaluation and Expressing the Uncertainty of NIST Measurement Results***, NIST TN-1297, MD, 1994.

[16] Johnson, A. N., Ricker, J., and Boyd, J., ***Computational Fluid Dynamic (CFD) Investigation of NIST's Scale-Model Smokestack Simulator***, Measurement Science Conference, Anaheim, CA 2013.